Layout: T3 Grey | Book ID: 627986_1_En | Book ISBN: 978-3-031-63936-4
Chapter No.: 72 | Date: 28-6-2024 | Time: 8:04 pm | Page: 1/12

Gamma Prime Precipitation in Cast and Wrought AD730® Superalloy

Jérôme Blaizot, Laurane Finet, Aurélien Chabrier, Alexandre Fornara, Matthieu Fage, Roufeida Remichi, Mickaël Dadé, and Michel Perez

Abstract

AD730® is a $\gamma - \gamma'$ polycrystalline superalloy which has γ/γ' been recently developed for future engine turbine discs. The γ' precipitation influences mechanical properties at the service temperature but also the kinetics of recrystallization during forging process. Consequently, a deep understanding and monitoring of γ' precipitation is required at each stage of the industrial process. The objective of this work is to understand the precipitation mechanism, determine the evolution of γ' size during cooling and isothermal heat treatments, and calibrate a model for the nucleation and growth of γ' during the ingot-to-billet conversion. The experimental analysis showed that water quenching at a cooling rate of 100 °C/s after a solution treatment at 1160 °C led to a fine and homogeneous γ' precipitation for which the average circle radius ranges from 10 to 20 nm. Then, samples were heat treated between 1000 and 1080 °C with various holding times to characterize and quantify the size of precipitates. The results were compared to the precipitation modeling using the in-house software PreciSo, a multi-class, Kampmann-Wagner Numerical precipitation model based on classical nucleation and growth theories. Even if the simulations of precipitation during isothermal heat treatments start with the correct initial radius, coarsening appears to occur slower than predicted by the simulations. This discrepancy is attributed to one simulation parameter, the diffusivity of solute elements, which needs to be improved to obtain a better fit with experimentations.

Keywords

γ/γ' Superalloy • γ' Precipitation • Modeling • Microstructure • AD730®

Introduction

To reduce the environmental impact of gas turbine engine, the maximum service temperature needs to be increased. To achieve these specifications, nickel-based superalloy AD730®[1] has been recently developed to be used for the future engine turbine discs. AD730® is a cast and wrought superalloy which exhibits good strength, creep and fatigue properties up to 750 °C [1]. AD730® is a $\gamma - \gamma'$ polycrystalline superalloy which could be manufactured at a lower cost than powder metallurgy superalloys. γ' precipitates provide the mechanical strength at the operating temperature and play a role on grain refinement during the forging process. γ' precipitation controls the final grain size and can slow down the kinetics of recrystallization due to the occurrence of fine and dense precipitates [2]. Heterogenous precipitation can lead to non-uniform grain distributions which strongly affect ultrasonic inspectability [3] and fatigue properties. To control the grain refinement, a deep understanding and monitoring of γ' precipitation is required at each stage of the industrial process.

The mechanisms of γ' precipitation during the first stages were studied, at the beginning, for single crystal nickel-based superalloys [4]. A schematic of the successive

J. Blaizot (✉) · L. Finet · A. Chabrier · A. Fornara · M. Fage · R. Remichi
Technical Division, Aubert & Duval, BP1, 63770 Les Ancizes, France
e-mail: jerome.blaizot@aubertduval.com

M. Dadé
ERAMET Ideas, 1 Avenue Albert Einstein, BP 120, 78193 TRAPPES, France

M. Perez
UMR CNRS 5510, Université de Lyon, INSA-Lyon, MATEIS, 69621 Villeurbanne, France

[1] AD730® is a registered trademark of Aubert and Duval.

J. Cormier et al. (eds.), *Superalloys 2024: Proceedings of the 15th International Symposium on Superalloys*, The Minerals, Metals & Materials Series, https://doi.org/10.1007/978-3-031-63937-1_72

Layout: T3 Grey | Book ID: 627986_1_En | Book ISBN: 978-3-031-63936-4
Chapter No.: 72 | Date: 28-6-2024 | Time: 8:04 pm | Page: 2/12

shape changes encountered during the structural evolution of a freely growing precipitate has been proposed by Grosdidier et al. [4]. The nucleation and growth of precipitates are driven by the reduction of global internal energy of the system according to the classic nucleation theory. The free growth of γ' precipitates leads to the following sequence of successive shape changes: sphere → cube → octocube → octodendrite → dendrite [4]. For AD730®, the precipitation mechanisms and kinetics of γ' particles during cooling from supersolvus and subsolvus temperatures were studied by differential thermal analysis and secondary electron microscopy by Masoumi et al. [5]. The γ' morphology evolves from a spherical shape at high cooling rates (120 °C/min) to butterfly shapes at low cooling rates (10 °C/min) due to strong interactions between precipitates and grain boundaries [6].

There is a strong coupling between γ' precipitation and the recrystallization front which evolve simultaneously during cooling. An interesting finding about this kind of coupling is the dissolution of γ' precipitates by the recrystallization front during post dynamic recrystallization [7]. More recently, the evolution of γ' precipitates was studied during the early stages of the industrial forging of AD730® [2]. A mix of continuous and discontinuous precipitation was observed and characterized after slow cooling at 10 °C/h from 1160 °C. Interestingly, it was observed that discontinuous precipitates inhibit the mechanism of recrystallization due to the small inter-precipitate spacing. Consequently, the development of a precipitation model could also help control recrystallization during the forging of a $\gamma - \gamma'$ polycrystalline superalloy. This kind of model needs to be implemented in a finite element framework to predict grain evolution and help design new forging routes [8].

There are several ways to model the precipitation depending on the time and lengths scales: Johnson–Mehl–Avrami-Kolmogorov equation [9], classical nucleation and growth theories, phase field, molecular dynamics and Monte-Carlo atomistic kinetic. This work focuses on a multi-class precipitation model based on the classical nucleation and growth theory [10–12] to reduce computational resources in comparison to other modeling approaches. Various investigations were conducted to model the γ' precipitation in $\gamma - \gamma'$ polycrystalline superalloy. In the René 65 superalloy, a model was used to predict the size of secondary γ' precipitation in relationship with the final mechanical properties [13]. A coarsening model was proposed by Masoumi et al. for AD730® to predict the γ' volume fraction and average size after various heat treatments [14]. This model considers the agglomeration of precipitates which plays an important role during the growth of γ' precipitates. Recently, a mean field model of precipitate agglomeration was proposed by Seret et al. [15] and used to predict the size distribution of γ' during cooling for AD730® [16]. For AD730®, it remains necessary to predict the distribution of γ' precipitates for various heat treatments and a broad range of precipitate sizes.

The objective of the present study is to understand the precipitation mechanism and calibrate a model for the nucleation and growth of γ' during ingot forging. The first step is to characterize γ' precipitates and determine the evolution of the γ' size during cooling and isothermal heat treatments. The second step is to predict the evolution of γ' precipitates for various heat treatments and compare with experimental results.

Material and Methods

a. Material and Experimental Plan

The material used in this study is a polycrystalline $\gamma - \gamma'$ nickel-based superalloy AD730®. The nominal chemical composition of this alloy is provided in Table 1. The ingot was triple melted by VIM (Vacuum Induction Melting), ESR (Electro Slag Remelting) and VAR (Vacuum Arc Remelting) processes. It is then homogenized before the upsetting and open die forging operations. Rectangular samples (10 × 40 mm) were cut from the resulting billet of 204 mm diameter.

In order to study the precipitation kinetics, a first solution heat treatment (HT1) is necessary to fully dissolve the precipitates. It is followed by water quenching to cool the samples as soon as possible. Then, isothermal aging heat treatments (HT2) are done at various temperatures to determine the nucleation and growth kinetics of precipitates as a function of temperature. In this case, the first supersolvus solution heat treatment (HT1) was done at 1160 °C for 4 h. This temperature is higher than the solvus temperature of γ' precipitates which is close to 1110 °C for AD730® [14]. Then, isothermal aging heat treatments (HT2) were done at 1000 °C, 1040 °C, and 1080 °C for various holding times from 1 to 24 h (Table 2). The maximum temperature deviation from the target is 10 °C for all heat treatments.

Table 1 Chemical composition of AD730® billet material

Element	Ni	Fe	Cr	Co	Mo	W	Al	Ti	Nb	C	B	Zr
Weight %	Bal	4	15.7	8.5	3.1	2.7	2.25	3.4	1.1	0.02	0.01	0.03

Layout: T3 Grey | Book ID: 627986_1_En | Book ISBN: 978-3-031-63936-4
Chapter No.: 72 | Date: 28-6-2024 | Time: 8:04 pm | Page: 3/12

Table 2 Isothermal heat treatments

First heat treatment (HT1)			Second heat treatments (HT2)		
Temperature (°C)	Holding time (h)	Cooling	Temperature (°C)	Holding time (h)	Cooling
1160 ± 10	4	Water quenching	1000 ± 10	1; 2; 4; 24	Air quenching
			1040 ± 10		
			1080 ± 10		

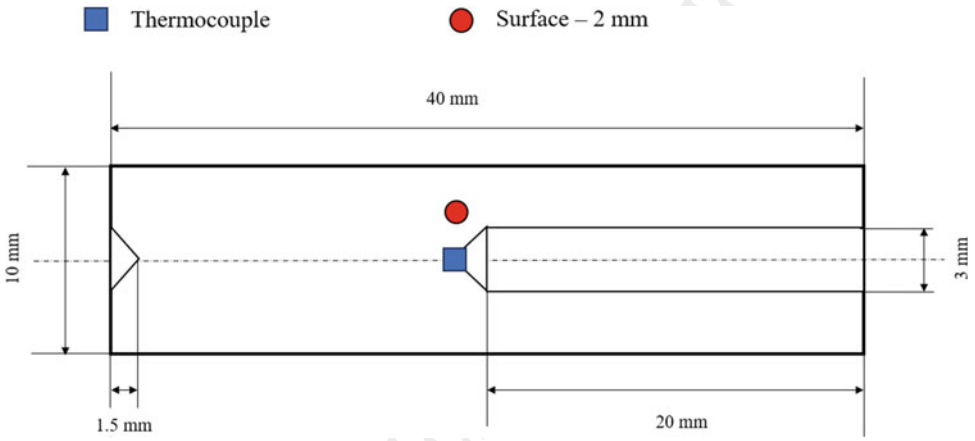

Fig. 1 Geometry of the rectangular sample used for the heat treatments (longitudinal median section)

b. Heat treatments

i. Sample design

The design of the samples aims to minimize the thermal gradient and control the cooling rate. To control the temperature during heat treatments, the samples were drilled to insert a thermocouple close to the center (Fig. 1). In a second step, finite-element simulations were performed to determine the thermal gradient and the variations of cooling rate during water quenching after the first heat treatment (HT1). These simulations were done with the FORGE®[2] software to compare the temperature profile at the center and at 2 mm below the surface.

ii. Finite-element simulations

For the water quenching model, heat transfer coefficients were defined as a function of the surface temperature in order to describe the main steps observed during calefaction, boiling, and convection. These coefficients also depend on the sample side considered: bottom, top, and lateral sides. The temperature profiles at the center and 2 mm from the surface were calculated and plotted along the recorded data in Fig. 2.

Firstly, it can be observed from Fig. 2 that there is a good agreement between the recorded and the simulated temperature profiles. Secondly, the temperature evolution at the center and at 2 mm from the surface exhibits the same slope. Therefore, the cooling rate is close to 100 °C/s for both positions in the precipitation temperature range (1050–850 °C). This hypothesis is consistent with the Biot number that can be estimated to be between 0.1 and 1.0. The Biot number is the ratio of the thermal resistance for conduction inside the sample to the resistance for heat transfer at the surface of the sample. A Biot number lower than 1 means that the thermal gradient is low.

c. Quantitative analysis of precipitates

There are several ways to determine quantitatively the size of γ' precipitates by scanning electron microscopy (SEM). The objective is to obtain high-contrast images between the γ matrix and the γ' precipitates without deteriorating the precipitation.

To study the γ' precipitation after water quenching from a super-solvus heat treatment (HT1), the samples were electrochemically polished under 35 V for 8 s in a methanol solution containing 10 vol. % of perchloric acid. γ' precipitates were characterized by High Resolution Scanning Electron Microscopy (HR SEM) operating at 5 kV and using secondary electron contrast (SE).

To quantify the γ' precipitation after isothermal heat treatments (HT2), the samples were prepared with a final polishing step using a colloidal silica suspension. γ' precipitates were characterized by HR SEM using backscattered electron contrast (BSE).

[2] FORGE® is a registered trademark of TRANSVALOR.

Layout: T3 Grey | Book ID: 627986_1_En | Book ISBN: 978-3-031-63936-4
Chapter No.: 72 | Date: 28-6-2024 | Time: 8:04 pm | Page: 4/12

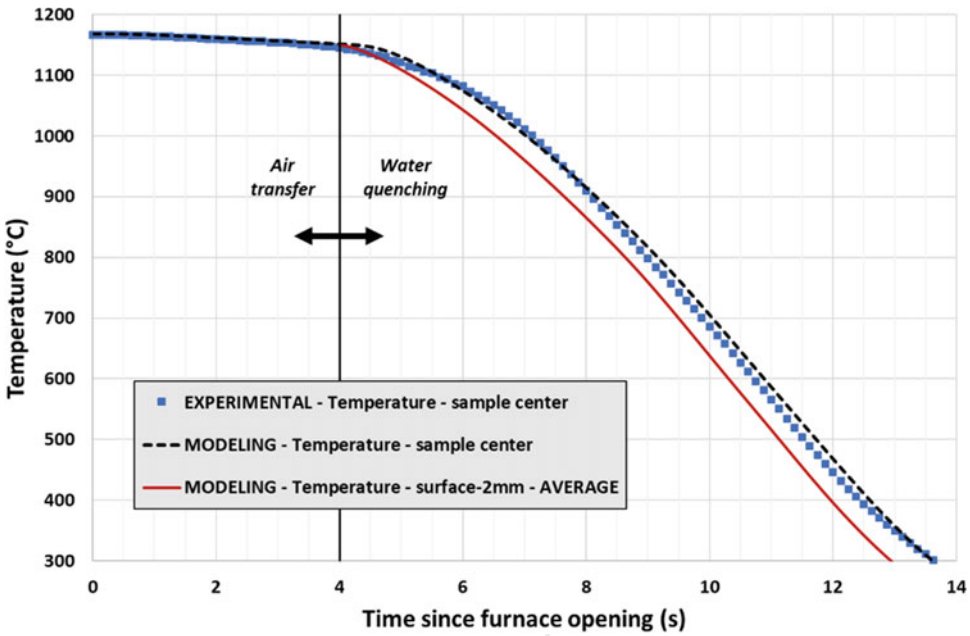

Fig. 2 Temperature profile during water quenching from 1160 °C (center of the sample in blue and 2 mm from the surface in red)

Experimental Results

a. Characterization of γ' precipitates after water quenching from super-solvus temperature

After full γ' precipitate dissolution at 1160 °C for 4 h, the microstructure is composed of equiaxed grains of 500 µm. Water quenching at a cooling rate of 100 °C/s (between 1050 and 850 °C) generated a fine and homogeneous population of γ' precipites with an average circle radius ranging between 10 and 20 nm (Fig. 3). The finest γ' precipitates with a radius below the equipment resolution (5 nm) were excluded from the analysis. The quick cooling leads to a very fine and dense precipitation because the density of precipitates is important (see section "Results and Discussion"b). At very low precipitate size, the spherical morphology is observed to minimize the interfacial energy [4].

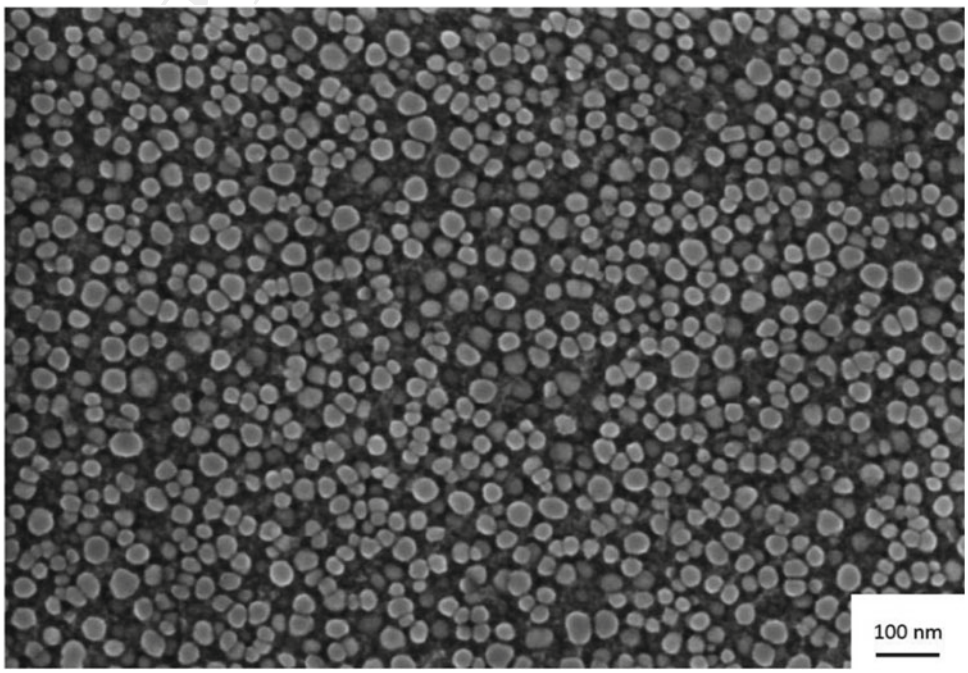

Fig. 3 HR SEM micrograph using secondary electron (SE) of γ' precipitates after a solution heat treatment at 1160 °C for 4 h followed by water quenching

Layout: T3 Grey | Book ID: 627986_1_En | Book ISBN: 978-3-031-63936-4
Chapter No.: 72 | Date: 28-6-2024 | Time: 8:04 pm | Page: 5/12

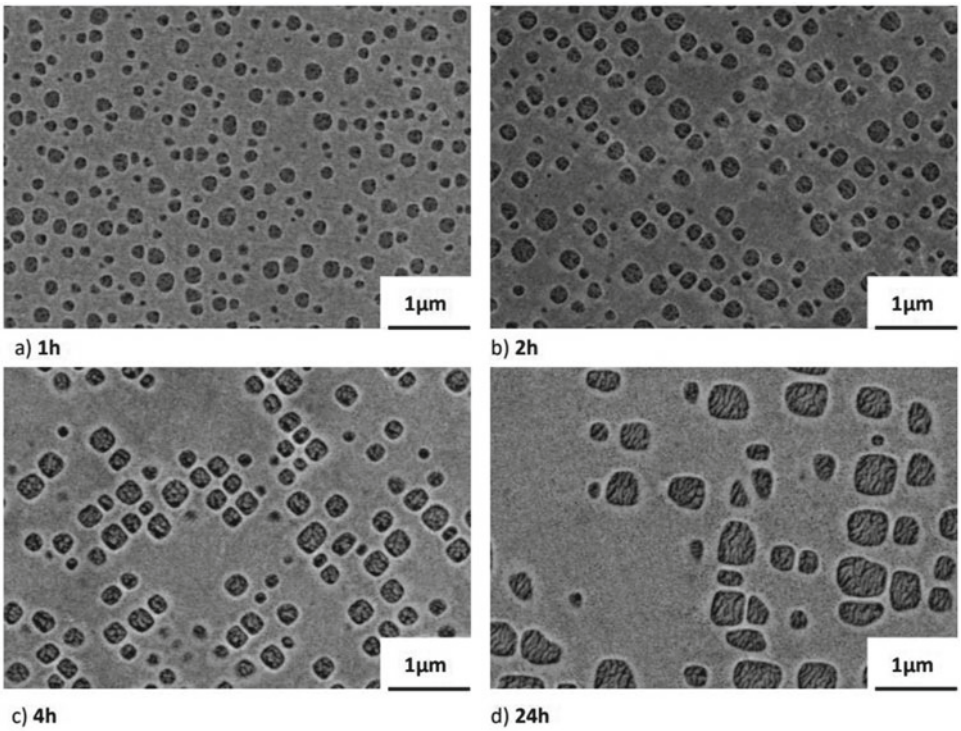

Fig. 4 HR SEM observations of γ' precipitates after heat treatment at 1040 °C (BSE)

Table 3 Average circle radius of γ' (nm) for the isothermal heat treatments

Temperature (°C)	Holding time (h)				
	1	2	4	24	
1000 ± 10	49 ± 5	60 ± 6	78 ± 7	130 ± 13	Average circle radius (nm)
1040 ± 10	68 ± 5	82 ± 5	103 ± 6	184 ± 17	
1080 ± 10	88 ± 13	115 ± 10	145 ± 11	229 ± 16	

b. Quantification of γ' precipitates during isothermal heat treatments

The size and morphology of γ' precipitates were characterized after heat treatment between 1000 and 1080 °C. γ' precipitates initially have a spheroidal appearance (Fig. 4a) that slowing transitions to cuboidal (Fig. 4b, c, and d). The transition from spherical to cubic morphology is due to the competition between interfacial and elastic contributions. As the precipitate volume increases, the elastic contribution becomes predominant consequently the cubic morphology is preferred [4]. The average circle radius was calculated after image analysis of at least four pictures using ImageJ (Table 3). The average equivalent circle radius of γ' precipitates will be compared with simulation results and literature data in section "Results and Discussion"c.

Modeling of γ' Precipitation

Precipitation was modeled using the inhouse software PreciSo [11, 12], a multi-class, Kampmann-Wagner Numerical (KWN) precipitation model [10] based on the classical nucleation and growth theory (details of the implementation in [17]). The methodology adopted in this work will be first explained. Then, the origin of all input parameters will be presented. Finally, modeling and experimental results will be compared and discussed.

Layout: T3 Grey | Book ID: 627986_1_En | Book ISBN: 978-3-031-63936-4
Chapter No.: 72 | Date: 28-6-2024 | Time: 8:04 pm | Page: 6/12

c. Classical Nucleation and Growth Theories

Nucleation

The nucleation rate dN/dt is the number of precipitates reaching the critical size r^* above which they are stable and grow:

$$\frac{dN}{dt} = N_0 Z \beta^* \exp\left[-\frac{\Delta G^*}{k_B T}\right] I(t) \quad (1)$$

where N_0 is the nucleation site number density, Z the Zeldovich factor, β^* the condensation rate, ΔG^* the nucleation energy barrier, k_B the Boltzmann constant, T the temperature (in Kelvin) and $I(t)$ the incubation time ($I(0) = 0$ and $I(\infty) = 1$). The nucleation energy barrier is the result of conflicting precipitate/matrix interfacial energy γ and precipitate driving force Δg (for spherical precipitates):

$$\Delta G^* = \frac{16}{3}\pi \frac{\gamma^3}{\Delta g^2} \quad (2)$$

The driving force Δg is computed from the solubility product $K(T)$ (a constant for a given precipitate in a given matrix depending only on temperature T):

$$\Delta g = \frac{k_B T}{v_m^{at}} \log\left[\frac{\prod (X_i)^{\varphi_i}}{K(T)}\right] \quad (3)$$

where X_i is the solute content of element i in the matrix, v_m^{at} is the atomic volume of the matrix, exponent φ_i is the amount of element i in the precipitate (e.g. $\varphi_{Ni} = 3$ for Ni3 (Ti0.5, Al0.5)).

Growth

The growth rate dr/dt is the stationary solution of the first Fick's diffusion law. For each diffusing chemical species i:

$$\frac{dr}{dt} = \frac{D_i}{r} \frac{X_i - X_i^e(r)}{\alpha X_i^p - X_i^e(r)} \quad (4)$$

where D_i is the diffusion coefficient of element i in Ni, X_i the far field mole fraction of element i, $\alpha = v_m^{at}/v_p^{at}$ is the ratio of matrix to precipitate atomic volume, X_i^p is the mole fraction of element i in the precipitate and $X_i^e(r)$ is the equilibrium fraction of element i at the interface between matrix and precipitate.

Additionally, these equilibrium fractions $X_i^e(r)$ are connected via the so-called Gibbs–Thomson equation, to the solubility product K of the precipitate and its radius r:

$$\prod \left(X_i^e\right)^{\varphi_i} = K(T) \exp\left[\frac{2(\sum \varphi_i)\gamma v_p^{at}}{r}\right] \quad (5)$$

Mass Balance

After the nucleation and growth stages, the mass balance is performed on all alloying elements, assuming that what remains in solid solution is the difference between alloying element content (X_i^0) and what is involved into precipitates:

$$X_i = \frac{X_i^0 - \alpha f X_i^p}{1 - \alpha f} \quad (6)$$

where f is the precipitate volume fraction.

Implementation

At each time step of the simulation, a new precipitate class j is created with population $N_j = \left(\frac{dN}{dt}\right)\Delta t$ and radius $R_j = r^*$. All existing precipitate classes grow according to $R_j(t + \Delta t) = R_j(t) + (dr/dt)\Delta t$, where dr/dt is the solution of the non-linear system formed by eqs. 4 and 5. Time step is adjusted to ensure smooth evolution of all simulation parameters and classes are managed to keep an accurate description of precipitate size distribution.

b. Modeling methodology

The aim of this approach is to model the evolution of $\gamma\prime$ precipitates assumed to be Ni3(Al0.5, Ti0.5) as a preliminary step. Carbides experimentally observed are assumed to be (Ti0.8, Nb0.2)C [14]. Chemistry of $\gamma\prime$ and carbides is very close to thermodynamic calculations using Thermo-Calc with TTNI8 database. For $\gamma\prime$, the number of elements is limited in the composition to reduce the calculation time. Then, Nb is not considered in $\gamma\prime$ as its amount is lower than for Al and Ti.

Three modeling stages were used to reproduce experimental features (Fig. 5):

Stage i: this stage is an isothermal treatment of 109 s at 1160 °C. It is performed to ensure full precipitation and coarsening of (Ti0.8,Nb0.2)C carbides up to a radius of approximatively 5 µm. These carbides have to be accounted for because they use part of Ti available for precipitation of γ'. They will remain active in stages j and k during which they will be able to grow or shrink, but no further nucleation will be allowed. This stage was done only numerically to take in consideration the MC carbide precipitation which appears during the solidification of the alloy.

Layout: T3 Grey | Book ID: 627986_1_En | Book ISBN: 978-3-031-63936-4
Chapter No.: 72 | Date: 28-6-2024 | Time: 8:04 pm | Page: 7/12

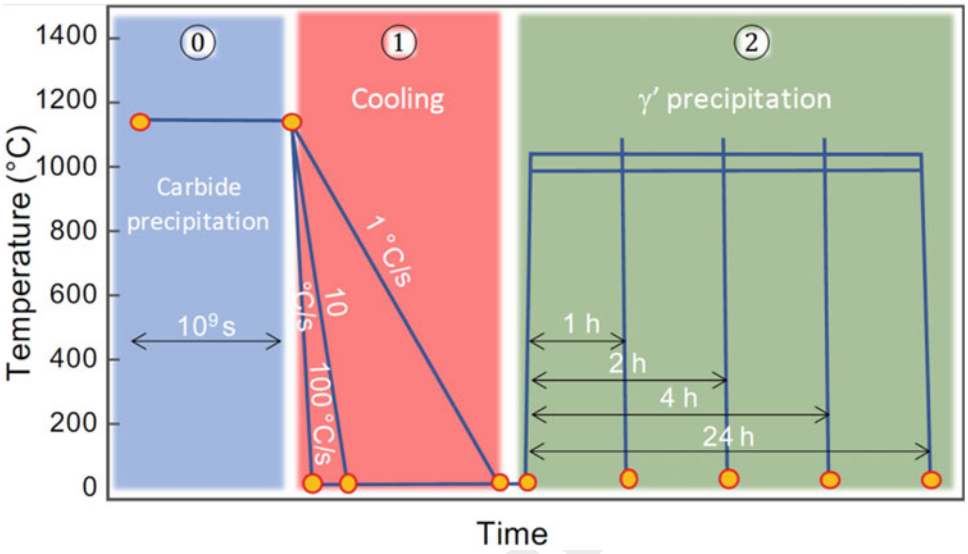

Fig. 5 Modeling methodology. Stage ι: precipitation of carbides at 1160 °C; stage φ: cooling at different cooling rates; stage κ: iso-thermal γ' precipitation

Stage j: this stage is a continuous cooling from 1160 °C to room temperature at various cooling rates (from 100 to 1 °C/s). This stage is performed to study the effects of cooling rate on γ' precipitation (HT1).

Stage k: this stage is an iso-thermal treatment of various duration (from 1 to 24 h) at temperatures of 1000, 1040, or 1080 °C. It is performed to compare precipitate size distribution evolution during experimental HT2 treatments.

At the end of each stage, precipitate size distributions (for carbides and $\gamma\prime$) are saved and used as initial distributions for the following stage.

c. Input parameters

For the modeling of γ' precipitation, some necessary data are quite difficult to measure for example, the diffusion coefficient of γ'-former elements in the γ matrix and the composition of the different phases at the target temperature to calculate the solubility product. For the present study, these data were obtained through calculations with the Thermo-Calc software (2023b release) and the TTNi 8 database [18].

Input parameters of the precipitation model are given in table 4. The solubility product for γ' phase and carbides is dependent on the concentration in the γ matrix of γ'-former and carbide-former elements respectively. Solubility product of carbides and $\gamma\prime$ has the form:

$$\log_{10}K(T) = \frac{C}{T^2} - \frac{A}{T} + B \tag{7}$$

where A, B, and C are constant derived from thermodynamic calculations using Thermo-Calc and the TTNI8 database.

The diffusion coefficients of all alloying elements are expressed through Eq. 8 [19]:

Table 4 Input parameters of precipitation model

Elements	Value	Unit	Ref.
$D_{0\mathrm{Al}}$	7.441×10^{-4}	m^2/s	MOBNI5
Q_{Al}	276.0	kJ/mol	MOBNI5
$D_{0\mathrm{Ti}}$	1.004×10^{-4}	m^2/s	MOBNI5
Q_{Ti}	258.6	kJ/mol	MOBNI5
$D_{0\mathrm{Nb}}$	1.070×10^{-4}	m^2/s	MOBNI5
Q_{Nb}	260.9	kJ/mol	MOBNI5
$D_{0\mathrm{C}}$	1.076×10^{-4}	m^2/s	MOBNI5
Q_{C}	172.4	kJ/mol	MOBNI5
Matrix			
$v_m^{at} = 1/N_0$	1.147×10^{-29}	m^3	
Carbides			
γ	0.22	J/m^2	Fitted
v_p^{at}	2.278×10^{-29}	m^3	
A	2.698×10^4	K	TTNI8
B	−5.793	–	TTNI8
C	-2.633×10^6	K2	TTNI8
$\gamma\prime$			
γ	0.12	J/m^2	Fitted
v_p^{at}	1.136×10^{-29}	m^3	
A	1.349×10^4	K	TTNI8
B	4.065	–	TTNI8
C	2.962×10^6	K2	TTNI8

$$D_i = D_{0i}\exp\left[-\frac{Q_i}{RT}\right] \tag{8}$$

where R is the ideal gas constant, D_{0i} (the pre-exponential factor) and Q_i (the activation enthalpy) are constant derived

Layout: T3 Grey | Book ID: 627986_1_En | Book ISBN: 978-3-031-63936-4
Chapter No.: 72 | Date: 28-6-2024 | Time: 8:04 pm | Page: 8/12

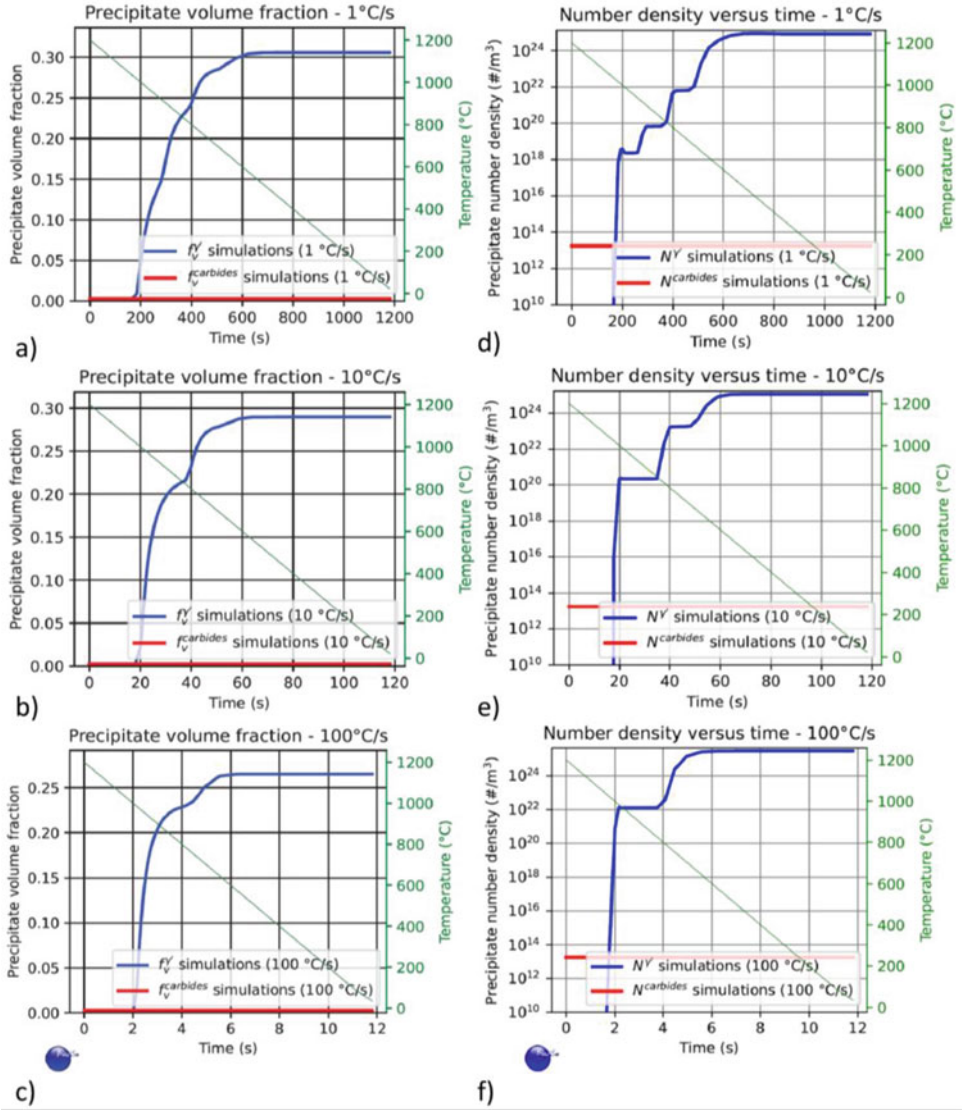

Fig. 6 Evolution of the volume fraction and number density for carbide and $\gamma\prime$ during cooling from 1160 °C to room temperature at 1 °C/s (**a**, **d**), 10 °C/s (**b**, **e**), and 100 °C/s (**c**, **f**) respectively

from calculations using Thermo-Calc with the MOBNI5 mobility database.

In this approach, the interfacial energy between γ and $\gamma\prime$ is the only fitted parameter and set to 0.12 J/m^2 to get the correct radius after the rapid cooling at 100 °C/s representative of HT1 cooling (Fig. 7). The fitted interfacial energy of γ' is close to values reported in literature for nickel-based superalloys (between 0.060 and 0.090 J/m^2 for nickel-based superalloys) [20]. The carbide interfacial energy is set to 0.22 J/m^2 in order to match the experimental size of carbides at the end of stage 0. Note that the matrix/carbide interfacial energy has almost no effect on all results since carbides do not evolve during stages 1 and 2.

Note that approximations are made on the stoichiometry and composition of the precipitated phases (γ' and carbides) and on the diffusion coefficients, which are considered fixed during the entire isothermal treatment. The reality is that chemical diffusion coefficients vary with changes in the matrix composition occurring during the growth of $\gamma\prime$ precipitates

Results and Discussion

a. Carbide precipitation at 1160 °C.

The first stage of these simulations aims at forming primary carbides with a radius of approximatively 5 µm. For that purpose, an isothermal simulated treatment of 109 s at 1160 °C was performed on a sample containing all alloying elements in solid solution. As expected, no precipitation of $\gamma\prime$ was observed during this treatment because 1160 °C is higher than the solvus temperature. This precipitation state will serve as input precipitation state for the stage φ: cooling at room temperature.

Layout: T3 Grey | Book ID: 627986_1_En | Book ISBN: 978-3-031-63936-4
Chapter No.: 72 | Date: 28-6-2024 | Time: 8:04 pm | Page: 9/12

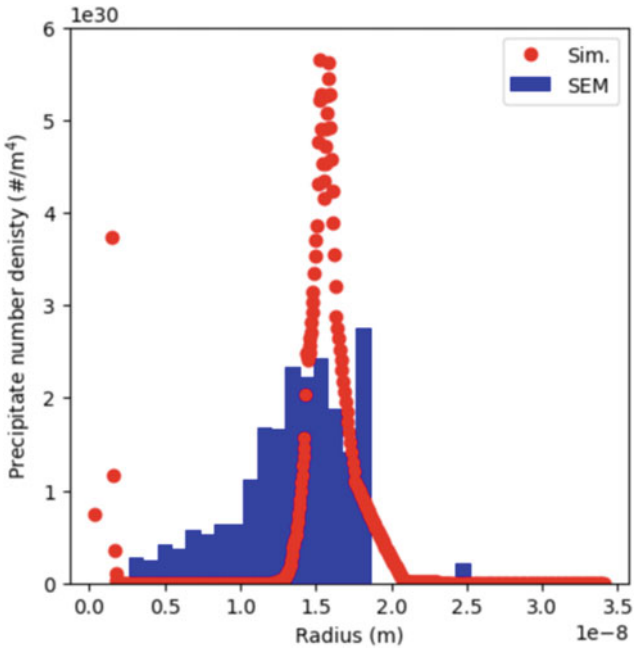

Fig. 7 Experimental and simulated $\gamma\prime$ precipitate size distribution after rapid cooling at 100 °C/s

b. Cooling at room temperature

Starting from the previous precipitation state (5 µm carbides and $\gamma\prime$ solutionized), cooling at different cooling rates (1, 10 and 100 °C/s) were simulated and compared. As explained before, a cooling rate at 100 °C/s from 1160 °C was used. The transfer time between the furnace and water tank is not considered for the simulation; consequently the simulation time (Fig. 6) is not the same as the experimental time (Fig. 2). The temperature decreases from 1160 °C to room temperature at a constant cooling rate in the simulation (Fig. 6). Whereas carbides do not evolve during cooling, massive precipitation of $\gamma\prime$ occurs. The lower is the cooling rate, the more $\gamma\prime$ precipitation occurs. This is due to the competition between driving force (that increases when temperature decreases) and diffusivity (that decreases when temperature decreases). At a low cooling rate (1 °C/s), the volume fraction of $\gamma\prime$ increases steadily (Fig. 6a) since the precipitation occurs in four stages (Fig. 6d). The volume fraction of $\gamma\prime$ increases sharply during cooling at 10 °C/s (Fig. 6b) and abruptly during cooling at 100 °C/s (Fig. 6c). Precipitation occurs in three stages at 10 °C/s (Fig. 6e) and in two stages at 100 °C/s (Fig. 6f). At approximatively 1000 °C, a first population of precipitates appears (low driving force and therefore large size). In the case of fast cooling, this first population constitutes the majority of precipitate volume fraction (Fig. 6c). Then, at lower temperature (between 800 and 600 °C), remaining solute atoms precipitate in the form of very numerous tiny precipitates (Fig. 6f).

The multi-stage precipitation leads to a bi-modal size distribution at 100 °C/s, as represented in Fig. 7. Simulated distribution resulting from fast cooling at 100 °C/s is compared to the experimental one resulting from cooling at the same rate. We can observe a good agreement between both distributions. Therefore, this distribution (in addition to the existing carbides that did not evolve during cooling) will serve as the initial distribution for the isothermal treatments performed in the next stage.

c. Isothermal precipitation treatments

After rapid cooling, the resulting carbide and $\gamma\prime$ precipitate size distribution is loaded as initial state and isothermal treatments are performed at 1000, 1040, and 1080 °C. Figure 8 shows the evolution of precipitate mean radii (carbides and $\gamma\prime$) versus time. After a transient time of approximately 1–10 s (depending on temperature), precipitates start to coarsen following a typical $R \propto t^{1/3}$ behavior.

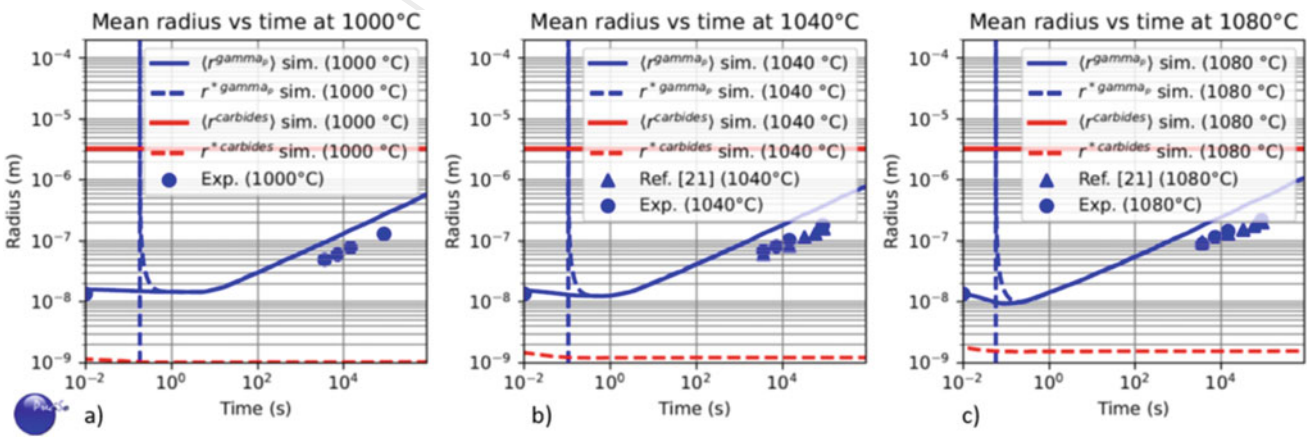

Fig. 8 Evolution of precipitate mean radii (carbides and $\gamma\prime$) versus time for isothermal treatments at 1000 °C (**a**), 1040 °C (**b**), and 1080 °C (**c**)

Layout: T3 Grey | Book ID: 627986_1_En | Book ISBN: 978-3-031-63936-4
Chapter No.: 72 | Date: 28-6-2024 | Time: 8:04 pm | Page: 10/12

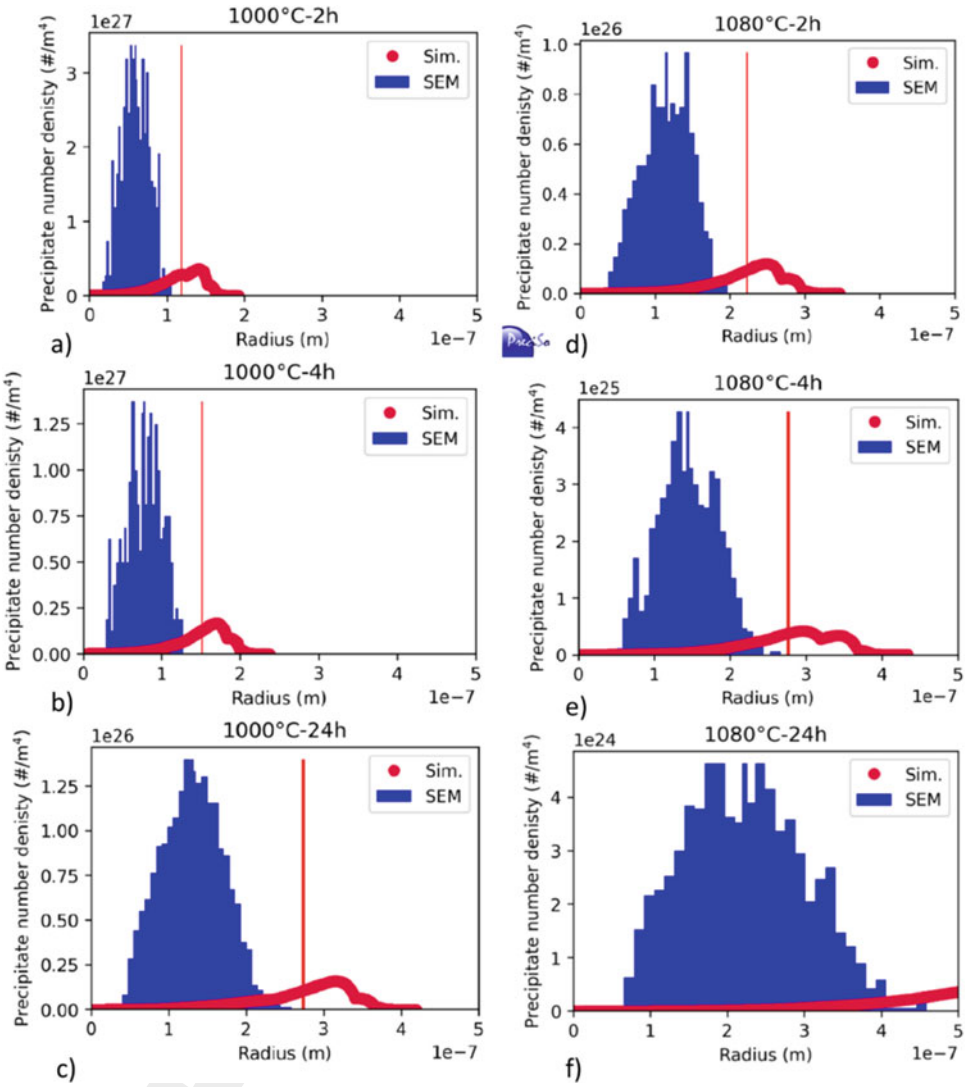

Fig. 9 Precipitate size distribution at 1000 °C (**a**: 2 h, **b**: 4 h, **c**: 24 h) and at 1080 °C (**d**: 2 h, **e**: 4 h, **f**: 24 h)

Simulations are compared with experimental values resulting from SEM image analysis. Even if the simulations start with the correct initial radius (Fig. 8), coarsening appears to occur slower than predicted by the simulations. Therefore, simulated distributions for various temperatures and times are larger than experimental ones (Fig. 9). The same trend is also observed for experimental results published in the literature [21]. Experimental coarsening appears to occur more slowly than predicted.

The only fitted parameter is the interfacial energy between γ and $\gamma\prime$ which was adjusted to 0.12 J/m^2 to obtain a good agreement between the experimental and simulated $\gamma\prime$ distributions after water quenching (HT1). The interfacial energy strongly influences nucleation which mainly occurs during cooling but has little impact on the growth rate of $\gamma\prime$ precipitates during isothermal heat treatments compared to the diffusivity of solute elements as can be seen in Eq. 4. The solute element diffusivity is the main parameter that can explain the discrepancy between simulations and experimentations during isothermal heat treatments. In order to validate this assumption, the diffusion coefficients of Al and Ti were multiplied by a factor 0.2 (by trial and error) and isothermal simulations were re-run. The evolution of the simulated radius at 1040 °C is similar to the values obtained experimentally (Fig. 10a). Moreover, a very good agreement between simulated and experimental $\gamma\prime$ precipitate distributions is obtained at 1040 °C (Fig. 10b and c). This leads to the conclusion that lowering the diffusivity of solute elements is necessary to get a better agreement on coarsening kinetics in this study.

Reasons for the deviation between experimental and simulated results may be due to approximations made for the input parameters, especially about the stoichiometry and composition of the precipitates. As a reminder, the $\gamma\prime$ precipitate composition was simplified, accounting for Ni, Al and Ti only but not Nb. The Nb content may play an

Layout: T3 Grey | Book ID: 627986_1_En | Book ISBN: 978-3-031-63936-4
Chapter No.: 72 | Date: 28-6-2024 | Time: 8:04 pm | Page: 11/12

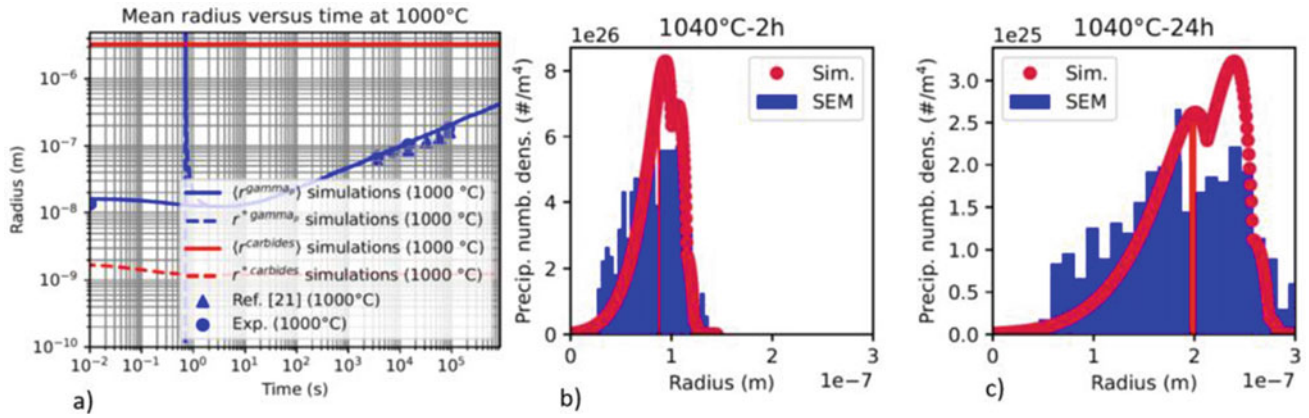

Fig. 10 Evolution of mean radius at 1040 °C and comparison between simulated and experimental $\gamma\prime$ precipitate distribution after multiplying the diffusion coefficient of Ti and Al by a factor 0.2

important role on their growth, as its diffusion coefficient is lower than Al and slightly lower than Ti according to the MOBNI5 database. Other elements could also have an influence on their growth, and if we go further, interstitial elements (like O, N, C) could lower the diffusion coefficients of Al, Ti and Nb [22]. For now, interstitial elements are not considered for the calculation of diffusion coefficients.

Conclusion

In this study, $\gamma\prime$ precipitation was characterized between 1000C and 1080 °C after cooling at 100 °C\s from 1160 °C. The size evolution of $\gamma\prime$ precipitates was quantified by HR SEM at various holding times from 1 to 24 h. Carbide and $\gamma\prime$ precipitations were modeled using inhouse software PreciSo to simulate the precipitation during the water quenching and the coarsening. The main conclusions are:

- Water quenching leads to a fine and homogeneous $\gamma\prime$ precipitation (between 10 and 20 nm for average circle radius).
- Precipitates coarsen following a typical $R \propto t^{1/3}$ behavior during isothermal heat treatments. A transition from spherical to cubical morphology is observed at 1040 °C.
- In this approach, the interfacial energy of γ' is the only fitted parameter and set to 0.12 J/m^2 to get the correct radius after the water quenching.
- The simulated growth rate of $\gamma\prime$ precipitates is over-estimated for each temperature which could be due to the diffusivity of solute element. A very good agreement between experimental and simulated results is obtained after dividing the diffusivity of solute element by a factor 5.

Deviation between experimental and simulated results may be due to approximations made for the input parameters, especially about the stoichiometry and composition of the precipitates. Isothermal simulations need to be rerun to investigate the influence of Nb element on the coarsening kinetics of $\gamma\prime$ precipitates. According to the several experimental results, this element would play an important role on the $\gamma\prime$ precipitation [21, 23]. Kinetics of nucleation and coarsening of $\gamma\prime$ can be also influenced by microsegregations of alloying elements which is not included in the current model.

Acknowledgements The authors thank Madeleine Bignon (CEMEF, Mines Paris PSL), Sophie Cazottes (Université de Lyon, INSA-Lyon, MATEIS), David Cardinaux, Christian Dumont, and Alexandre Devaux (Aubert and Duval) for the fruitful discussions as well as Guillaume Burlot (P' Institut) for the access to the comparative data.

References

1. Devaux, A., Picqué, B., Gervais, M. F., et al. AD730™-A New Nickel-Based Superalloy for High Temperature Engine Rotative Parts. Superalloys 2012, 2012, p. 911–919.
2. Coyne-Grell, A., Blaizot, J., Rahimi, S., et al. Evolution of γ′ precipitation during the early stages of industrial forging of a nickel-based superalloy. Metallurgical and Materials Transactions A, 2023, vol. 54, no 5, p. 2022–2036.
3. Thebault, J. Etudes expérimentale et numérique des mécanismes de déformation et de recristallisation de l'UDIMET 720 lors du forgeage. Relations entre la microstructure et la perméabilité aux ultrasons. 2009. Doctoral dissertation. Ecole Centrale Paris.
4. Grosdidier, T., Hazotte, A., and SIMON, A. Precipitation and dissolution processes in γ/γ′ single crystal nickel-based superalloys. Materials Science and Engineering: A, 1998, vol. 256, no 1-2, p. 183–196.
5. Masoumi, F., Shahriari, D., Jahazi, M., et al. Kinetics and Mechanisms of γ′ Reprecipitation in a Ni-based Superalloy. Scientific reports, 2016, vol. 6, no 1, p. 28650.

Layout: T3 Grey | Book ID: 627986_1_En | Book ISBN: 978-3-031-63936-4
Chapter No.: 72 | Date: 28-6-2024 | Time: 8:04 pm | Page: 12/12

6. Atrazhev, V. V., Burlatsky, S. F., Dmitriev, D. V., et al. The mechanism of grain boundary serration and fan-type structure formation in Ni-based superalloys. Metallurgical and Materials Transactions A, 2020, vol. 51, p. 3648–3657.
7. Seret, A., Moussa, C., Bernacki, M., et al. On the coupling between recrystallization and precipitation following hot deformation in a γ-γ' nickel-based superalloy. Metallurgical and Materials Transactions A, 2018, vol. 49, p. 4199–4213.
8. Bernacki, M., Bozzolo, N., de Micheli, P., et al. Numerical Modeling of Recrystallization in a Level Set Finite Element Framework for Application to Industrial Processes. 2019.
9. William, J. et Mehl, R. Reaction kinetics in processes of nucleation and growth. Trans. Metall. Soc. AIME, 1939, vol. 135, p. 416–442.
10. Wagner, R., Kampmann, R., et Voorhees, P. W. Homogeneous second-phase precipitation. Phase transformations in materials, 2001, p. 309–407.
11. Perez, M., Dumont, M., et Acevedo-Reyes, Daniel. Implementation of classical nucleation and growth theories for precipitation. Acta Materialia, 2008, vol. 56, no 9, p. 2119–2132.
12. Perez, M., Dumont, M., et Acevedo-Reyes, D. Corrigendum to¨ Implementation of classical nucleation and growth theories for precipitation'[Acta Materialia 56 (2008) 2119–2132]. Acta Materialia, 2009, vol. 57, no 4, p. 1318–1318.
13. Wessman, A. E. Physical Metallurgy of Rene 65, a Next-Generation Cast and Wrought Nickel Superalloy for use in Aero Engine Components. 2016. Doctoral dissertation. University of Cincinnati.
14. Masoumi, F., Jahazi, M., Shahriari, D., et al. Coarsening and dissolution of γ′ precipitates during solution treatment of AD730™ Ni-based superalloy: Mechanisms and kinetics models. Journal of Alloys and Compounds, 2016, vol. 658, p. 981–995.
15. Seret, A., Moussa, C., Bernacki, M., et al. A mean field model of agglomeration as an extension to existing precipitation models. Acta Materialia, 2020, vol. 192, p. 40–51.
16. Seret, A. Influence de la mise en forme sur les cinétiques de précipitation durcissante dans les superalliages base nickel Inconel® 625 et AD730™. 2019. Doctoral dissertation. Université Paris sciences et lettres.
17. Toffolon-Masclet, C., Perron, A., Mazères, B., et al. Computational kinetics: application to nuclear materials. Comprehensive Nuclear Materials, 2020, p. 850–880.
18. Andersson, J.-O., Helander, T., Höglund, L., et al. Thermo-Calc & Dictra, computational tools for materials science. Calphad, 2002, vol. 26, no 2, p. 273–312.
19. Mehrer, H. et Stolica, N. Landolt-Börnstein New Series Group III, Crystal and Solid State Physics, Vol. 26, Diffusion in Solid Metals and Alloys. 1990.
20. Li, X., Saunders, N., et Miodownik, A. P. The coarsening kinetics of γ′ particles in nickel-based alloys. Metallurgical and Materials Transactions A, 2002, vol. 33, p. 3367–3373.
21. Burlot, G. Formation des zones appauvries en précipitation γ'secondaire aux abords des joints de grains et impact sur les propriétés mécaniques des superalliages base nickel γ/γ'. 2023. Doctoral dissertation. ISAE-ENSMA Ecole Nationale Supérieure de Mécanique et d'Aérotechique-Poitiers.
22. Ter-Ovanessian, B., Berrest, C., Deleume, J., et al. Influence of interstitials content on the diffusion of Niobium in alloy 718. In: Defect and Diffusion Forum. Trans Tech Publications Ltd, 2009. p. 161–166.
23. Smith, G. D., Patel, S. J. The role of niobium in wrought precipitation-hardened nickel-base alloys. *Superalloys*, 2005, vol. 718, p. 625–706.